Reduced-dimensional vibrational models of the water dimer

Emil Vogt,[1] Irén Simkó,[2,3] Attila G. Császár,[2,3] and Henrik G. Kjaergaard[1, a)]

[1)] *Department of Chemistry, University of Copenhagen, Universitetsparken 5, DK-2100 Copenhagen Ø, Denmark*

[2)] *Laboratory of Molecular Structure and Dynamics, Institute of Chemistry, ELTE Eötvös Loránd University, Pázmány Péter sétány 1/A, H-1117 Budapest, Hungary*

[3)] *MTA-ELTE Complex Chemical Systems Research Group, P.O. Box 32, H-1518 Budapest 112, Hungary*

(Dated: 2 March 2022)

A novel model based on the finite-basis representation (FBR) of a vibrational Hamiltonian expressed in internal coordinates, is developed. The model relies on a many-mode, low-order expansion of both the kinetic energy operator and the potential energy surface (PES). Polyad truncations and energy ceilings are used to control the size of the vibrational basis, to facilitate accurate computations of the OH stretch and HOH bend intramolecular transitions of the water dimer, $(H_2{}^{16}O)_2$. Advantages and potential pitfalls of the applied approximations are highlighted. The importance of choices related to the treatment of the kinetic energy operator in reduced-dimensional calculations, as well as the accuracy of different water dimer PESs, are discussed. A range of different reduced-dimensional computations are performed to investigate the wavenumber shifts in the intramolecular transitions caused by the coupling between the intra- and intermolecular modes. With the use of symmetry, full 12-dimensional vibrational energy levels of the water dimer are calculated, predicting accurately the experimentally observed intramolecular fundamentals. It is found that one can also predict accurate intramolecular transition wavenumbers for water dimer by combining a set of computationally inexpensive reduced-dimensional calculations, thereby guiding future effective-Hamiltonian treatments.

I. INTRODUCTION

For more than half a century, vibrational spectroscopy of the water dimer, $(H_2O)_2$, has been of interest from both experimental[1–9] and theoretical[10–29] aspects. In the dimer, the H_2O monomers are held together by an $OH\cdots O$ hydrogen bond, considered to be the archetype of hydrogen bonds.[30] Within the many-body-expansion approach, the interaction of the two water monomers provide the leading contribution to potential energy surfaces (PES) of larger water clusters.[18,29]

Similar to other weakly-bound complexes, understanding the low-energy states of the water dimer is complicated by large-amplitude motions and, in particular, by complicated splitting patterns caused by low-energy barriers hindering these motions. Developing the ability to compute these observable splittings has been an important goal of theoretical and computational spectroscopy.[14,27,31,32] For water dimer, there are eight versions[32] of its equilibrium structure, of C_s point-group symmetry, if the possibility to break the four covalent OH bonds is ignored. The eight versions, corresponding to different numbering of the identical nuclei, can be interconverted by so-called "tunneling" rearrangements, defining "donor-tunneling", "acceptor-tunneling", and "donor-acceptor interchange" paths.[32] The low-energy vibration-rotation-tunneling (VRT) states of the water dimer are sensitive to minor changes in the PES; thus, they provide important checks for modeling efforts.[12] The benchmark of computed line lists against experimentally observed transition wavenumbers provides another accurate measure of the quality of the PES. As a result, there are several studies[12,20] which have been designed to observe and assign VRT states. Due to its importance and its complex nuclear dynamics, different theoretical and computational approaches, including variational(-type) nuclear-dynamics computations, have been tested for water dimer. The HBB,[16] HBB2,[17,18] WHBB,[18] MB-pol,[20] and CCpol-8sf[19,23] PESs are examples of water-dimer potentials that allow for displacements along all 12 vibrational degrees of freedom (DoF). Accurate VRT levels have been computed with each of these PESs.

Computation of VRT states is reported in Ref. 19, based on the CCpol-8sf PES (which was renamed to CCpol-8sfIR[2012] in Ref. 23). The authors of

[a)] Corresponding author.
hgk@chem.ku.dk

Ref. 19 used a (6+6)-dimensional (6D+6D) adiabatic approach, in which the six high-energy (small-amplitude) intramolecular DoFs were separated from the six low-energy (large-amplitude) intermolecular DoFs. For the water dimer, and for its fully deuterated analogue, this adiabatic approach resulted in accurate VRT energy levels.[19] At the same time, relatively large discrepancies from experiment were observed for the high-energy intramolecular transitions. The source of these discrepancies was not determined. More recently, numerically exact 12-dimensional (12D) calculations of the VRT levels, also based on the CCpol-8sf PES, were performed up to the region of the HOH bend states.[27] The (6D+6D) and 12D results were in excellent agreement with each other and with experiments for the low-lying intermolecular energy levels, confirming that the adiabatic approximation is excellent in the low-energy region.[19,27] However, large differences (up to 11 cm^{-1}) between the 12D and (6D+6D) calculations were obtained for the bending fundamentals, implying a breakdown of the adiabatic approximation for the intramolecular transitions. Due to the rapidly increasing density of states, the 12D calculations could not be extended to the region of the OH-stretch fundamentals.[27]

Here, the focus is not on the low-energy VRT states but rather on a related problem, the modeling of OH stretch and HOH bend *intramolecular* vibrational transitions of the water dimer. The formation of the hydrogen bond redshifts and increases the intensity of the bound OH stretch, OH_b, fundamental transition. These hydrogen bond characteristics were captured in the early anharmonic local mode effective Hamiltonian calculations.[13,33,34] Later, the inclusion of intermolecular low-energy modes that partially break the hydrogen bond were found to affect the size of the redshift.[22,24,35] As a consequence, to calculate accurate intramolecular transitions with an effective Hamiltonian, one needs a good description of both the intramolecular and intermolecular modes, as well as the coupling between the two sets of modes. However, it is not obvious which type of approximations are suitable to calculate accurate intramolecular transitions from an effective Hamiltonian.

To address this question, we have developed a novel, flexible finite-basis representation (FBR) model based on a many-mode expansion of both the PES and the **G** matrix elements in the vibrational kinetic energy operator in internal coordinates. The model and the associated code is termed VibMEMIC, in reference to its main characteristics: **Vib**rational **M**any-mode **E**xpansion **M**odel in **I**nternal **C**oordinates. With VibMEMIC, we perform a set of reduced-dimensional calculations to investigate the transition wavenumber shifts caused by the interaction between the intramolecular and intermolecular modes. Results are presented both for VibMEMIC, as well as from computations performed with a discrete-variable-representation-based model, GENIUSH (GENIUSH stands for **Ge**neral code with **N**umerical, **I**nternal-coordinate, **U**ser-**S**pecified **H**amiltonians),[36–38] in which neither the PES nor the kinetic energy operator are approximated. We used a newly calculated CCSD(T)-F12a/cc-pVTZ-F12 PES, abbreviated as F12, with VibMEMIC, and the CCpol-8sfIR[19,23] and the MB-pol[20] surfaces with GENIUSH. We discuss the degree to which the transition wavenumber shifts caused by each of the low-energy intermolecular modes are additive. In addition, we provide accurate intramolecular transition wavenumbers from full-dimensional 12D computations performed with VibMEMIC. We show that not only do the reduced-dimensional calculations provide physical insight into the transition wavenumber shifts, they can also predict the intramolecular transitions rather accurately.

II. VIBMEMIC

The VibMEMIC model was developed for the purpose of calculating accurate stretch and bend intramolecular transitions for hydrogen bound complexes. Most previous vibrational models focus either on the low-energy intermolecular modes or on the high-energy intramolecular modes. In earlier work, the coupling between the two sets of modes have typically been approximated or neglected. Models based on an adiabatic separation of the two sets of modes have proven useful for describing the affect of the intramolecular modes on the intermolecular transitions, however, this separation has been shown to work less well for the intramolecular transitions.[19,27] Models built on effective Hamiltonians can yield accurate intramolecular transitions for hydrogen bound complexes, but often these types of models rely to some extend on cancellation of error. Their accuracy depends on both the type of transitions and on the validity of the introduced approximation for the specific complex in question.[22,24] The VibMEMIC model may be viewed as an extension of the effective Hamiltonian approaches to include a more accurate description of the low-energy intermolecular modes and their coupling with the high-energy intramolecular mode. Alternatively, it can be viewed as a reduction of the exact or near-exact models, typically used for the intermolecular modes, to facilitate calculations includ-

ing more vibrational modes. In Section II A, the general framework for constructing the Hamiltonian in the VibMEMIC model is introduced. In Sections II B-II E, we describe the employed coordinate system for water dimer, general symmetry aspect of water dimer and how symmetry is utilized, how the basis is truncated, and the employed notation for the intramolecular transitions, respectively.

A. The Hamiltonian

The current version of VibMEMIC can solve only the vibrational Schrödinger equation, *i.e.*, rotations are not treated. The M-dimensional vibrational Hamiltonian is expressed in the form derived by Podolsky:[39]

$$\hat{H} = \frac{1}{2}\sum_{ij}^{M} \tilde{g}^{-1/4}\hat{p}_i^{\dagger} G_{ij} \tilde{g}^{1/2}\hat{p}_j\tilde{g}^{-1/4} + V, \tag{1}$$

where M is the number of vibrational modes ($M \leq 3N-6$(5), and N is the number of atoms in the molecule), $\hat{p}_i = -\mathrm{i}\hbar\frac{\partial}{\partial q_i}$, with q_i being the i'th coordinate, and $\tilde{g} = \det(\mathbf{g})$. The $3N \times 3N$-dimensional $\mathbf{g}$ and $\mathbf{G}$ matrices (covariant and contravariant metric tensor, respectively) can be expressed as[40]

$$g_{ij} = \sum_{\alpha=1}^{3N} m_\alpha \frac{\partial x_\alpha}{\partial q_i}\frac{\partial x_\alpha}{\partial q_j} \;\Leftrightarrow\; \mathbf{g} = \mathbf{J}\mathbf{M}\mathbf{J}^T \tag{2}$$

and

$$G_{ij} = \sum_{\alpha=1}^{3N} \frac{1}{m_\alpha}\frac{\partial q_i}{\partial x_\alpha}\frac{\partial q_j}{\partial x_\alpha} \;\Leftrightarrow\; \mathbf{G} = \mathbf{g}^{-1}, \tag{3}$$

where the sum is over all Cartesian coordinates of the atoms of the molecule, m_α denotes the associated masses, the q_i coordinates include all vibrational, rotational, and translational coordinates, $\mathbf{J}$ is the Jacobian matrix ($J_{i\alpha} = \frac{\partial x_\alpha}{\partial q_i}$), and $M_{\alpha\beta} = m_\alpha\delta_{\alpha\beta}$ is the mass matrix. The matrix $\mathbf{G}$ is obtained by inverting $\mathbf{g}$, with elements of the Jacobian calculated using the finite-difference method. The Jacobian is of size $3N \times 3N$, and a full internal-coordinate definition, including the three rotational and three translational coordinates, is therefore required even for the reduced-dimensional vibrational models. The volume element of integration is $d\tau = dq_1 dq_2 ... dq_M$ (Wilson's normalization), for which the $\hat{p}_i$ operator is Hermitian. We use $\tilde{g} = \tilde{J}^2\tilde{M}$ [Eq. (2)], and write the Podolsky form of the Hamiltonian as

$$\hat{H} = \frac{1}{2}\sum_{ij}^{M} \tilde{J}^{-1/2}\hat{p}_i^{\dagger} G_{ij} \tilde{J}\hat{p}_j\tilde{J}^{-1/2} + V. \tag{4}$$

In reduced dimmentional models where $M < 3N-6$, there are constrained vibrational coordinates. These constraints can be taken into account by either deleting the corresponding rows and columns of $\mathbf{g}$ and then inverting it to obtain $\mathbf{G}$, or by inverting the full $\mathbf{g}$ matrix and deleting the corresponding rows and columns of $\mathbf{G}$. The vibrational basis functions in VibMEMIC are defined as products of eigenfunctions of 1D Hamiltonians ($\hat{h}_i$). These 1D Hamiltonians describe each mode as being decoupled from the remaining vibrational modes,

$$\hat{h}_i = \frac{1}{2}\tilde{J}^{-1/2}\hat{p}_i^{\dagger} G_{ii} \tilde{J}\hat{p}_i\tilde{J}^{-1/2} + V_i^{(1\mathrm{D})}(q_i), \tag{5}$$

where G_{ii} is evaluated at the reference value of all other vibrational coordinates and $V_i^{(1\mathrm{D})}(q_i)$ is the PES along the ith mode from the reference geometry. In Eqs. (4) and (5), the rotational and translational part of the determinant of the Jacobian can be excluded as the $\hat{p}_i$ (and $\hat{p}_j$) operator only operates on the vibrational coordinates. The vibrational part of the absolute value of the determinant of the Jacobian can be expressed as $|\tilde{J}_{\mathrm{vib}}| = \prod_{k=1}^{N-1} r_k^2 \prod_{l=1}^{N-2}\sin(\theta_l)$, where r is a bond length and θ is an azimuthal-type angle ($0 \leq \theta \leq \pi$).[41]

The Jacobian does not depend on the dihedral angles ($0 \leq \phi \leq 2\pi$), and the 1D Hamiltonian for a dihedral coordinate is simply

$$\hat{h}_i = \frac{1}{2}\hat{p}_i^{\dagger} G_{ii} \hat{p}_i + V_i^{(1\mathrm{D})}(q_i), \tag{6}$$

where we use a basis set of sine and cosine functions ($\{\chi(q_i)\} = \{(2\pi)^{-1/2}, \pi^{-1/2}\cos(q_i\cdot n), \pi^{-1/2}\sin(q_i\cdot n)\}$, with $n = 1, 2, ...$), and define the derivatives of these functions with respect to the coordinate as $\chi_l'(q_i) \equiv \frac{\partial\chi_l(q_i)}{\partial q_i}$.

For an azimuthal angle, the 1D Hamiltonian is

$$\hat{h}_i = \frac{1}{2}\sin^{-1/2}(q_i)\hat{p}_i^{\dagger} G_{ii}\sin(q_i)\hat{p}_i\sin^{-1/2}(q_i) + V_i^{(1D)}(q_i) \tag{7}$$

where we use a basis set of associated Legendre polynomials ($P_l^m(z)$ with $m = 0$), parameterized in terms of $z = \cos(q_i)$. Matrix elements of this Hamiltonian are now expressed as

$$\begin{aligned}\langle k|h_i|l\rangle = &\frac{-\hbar^2}{2}\int_0^\pi \chi_k'(q_i)G_{ii}\chi_l'(q_i)dq_i \\ &+ \int_0^\pi \chi_k(q_i)V_i^{(1D)}(q_i)\chi_l(q_i)dq_i\end{aligned} \tag{8}$$

where $\chi_l(q_i) = N_l\sin^{1/2}(q_i)P_l^0(\cos(q_i))$, with the normal-

ization constant $N_l = \left(l + \frac{1}{2}\right)^{1/2}$, and we define

$$\chi'_l(q_i) \equiv N_l \sin^{1/2}(q_i) \frac{\partial P_l^0(\cos(q_i))}{\partial q_i} \tag{9}$$
$$= \frac{N_l \cdot l}{\sin^{1/2}(q_i)} \cdot \left[\cos(q_i) \cdot P_l^0(\cos(q_i)) - P_{l-1}^0(\cos(q_i))\right].$$

Note that for azimuthal angles the $\chi'_l(q_i)$ functions are not the derivative of the $\chi_l(q_i)$ functions with respect to the coordinate as they were defined for dihedral angles. However, the $\chi'_l(q_i)$ functions are chosen to satisfy Eq. 8 in both cases. The associated Legendre polynomials are orthogonal with respect to the volume element of integration, $d\tau = \sin(q_i)dq_i$; thus, making the $\chi_l(q_i)$ functions orthonormal with respect to the volume element of integration, $d\tau = dq_i$

$$\int_0^\pi \chi_k(q_i)\chi_l(q_i)dq_i \tag{10}$$
$$= N_k N_l \int_0^\pi P_k^0(\cos(q_i)) P_l^0(\cos(q_i)) \sin(q_i) dq_i = \delta_{kl}$$

Associated Legendre polynomials with $m = 0$ are also used to solve the 1D Schrödinger equation for the stretches, analogous to what have just been shown for azimuthal angles, but with $q_i \rightarrow (q_i - \min(q_i)) \frac{\pi}{\max(q_i) - \min(q_i)}$.

For stretches and bends, we use Gauss–Legendre quadrature, and for dihedrals, we use Clenshaw–Curtis quadrature, both with a total of 101 points. In Table S1, we show the displacement ranges used for each internal coordinate. We store the 1D eigenfunctions;

$$\psi_v(q_i) = \sum_l c_{vl} \chi_l(q_i) \tag{11}$$

where c_{vl} is the l'th coefficient of the v'th eigenfunctions obtained from diagonalizing the 1D Hamiltonian, and also the functions;

$$\psi'_v(q_i) = \sum_l c_{vl} \chi'_l(q_i) \tag{12}$$

Evaluating elements of the M-dimensional kinetic energy operator with the $\psi'_v(q_i)$ functions has the advantage of removing the $\tilde{J}$ terms in the Podolsky Hamiltonian. For example, one kinetic energy matrix element between states that depend on both an azimuthal angle (q_i) and a dihedral angle (q_j) is:

$$\frac{1}{2} \int_{q_i^{\min}}^{q_i^{\max}} \int_{q_j^{\min}}^{q_j^{\max}} \psi_v(q_i)\psi_u(q_j) T_{ij} \psi_{v'}(q_i)\psi_{u'}(q_j) dq_i dq_j \tag{13}$$
$$= \frac{-\hbar^2}{2} \int_{q_i^{\min}}^{q_i^{\max}} \int_{q_j^{\min}}^{q_j^{\max}} \psi'_v(q_i)\psi_u(q_j) G_{ij} \psi_{v'}(q_i)\psi'_{u'}(q_j) dq_i dq_j$$

where $T_{ij} = \frac{1}{2}\tilde{J}^{-1/2}\hat{p}_i^\dagger G_{ij} \tilde{J} \hat{p}_j \tilde{J}^{-1/2}$ and $q_i^{\min}$ and $q_i^{\max}$ are the minimal and maximal values of the q_i coordinate. Equation (13) can be verified from the definitions of $\psi'_v(q_i)$, $\chi'_l(q_i)$ and $\tilde{J}_{\text{vib}}$, all of which have known analytical expressions.

To evaluate integrals needed to solve the M-dimensional Schrödinger equation, both the elements of the **G** matrix and the PES are represented with a many-mode expansion, truncated at third order.

$$V(q_1, q_2, ..., q_M) = V(q_1^{\text{ref}}, q_2^{\text{ref}}, ..., q_M^{\text{ref}}) \tag{14}$$
$$+ \sum_i^M V_i^{\text{1D}}(q_i) + \sum_{i<j}^M V_{ij}^{\text{2D}}(q_i, q_j) + \sum_{i<j<k}^M V_{ijk}^{\text{3D}}(q_i, q_j, q_k)$$

with

$$V_i^{\text{1D}}(q_i) = V(q_1^{\text{ref}}, q_2^{\text{ref}}, ..., q_i, ...q_M^{\text{ref}}) - V(q_1^{\text{ref}}, q_2^{\text{ref}}, ..., q_M^{\text{ref}}) \tag{15}$$

and

$$V_{ij}^{\text{2D}}(q_i, q_j) = V(q_1^{\text{ref}}, q_2^{\text{ref}}, ..., q_i, ..., q_j, ...q_M^{\text{ref}}) \tag{16}$$
$$- V(q_1^{\text{ref}}, q_2^{\text{ref}}, ..., q_M^{\text{ref}}) - V_i^{\text{1D}}(q_i) - V_j^{\text{1D}}(q_j)$$

and likewise for $V_{ijk}^{\text{3D}}(q_i, q_j, q_k)$, i.e., with $V(q_1^{\text{ref}}, q_2^{\text{ref}}, ..., q_M^{\text{ref}})$, the 1D and the 2D surfaces involving the i'th, j'th, and k'th mode subtracted from the 3D cut of the full PES from the reference geometry.

In this work, a new CCSD(T)-F12a/cc-pVTZ-F12[42,43] (abbreviated as F12) PES was calculated with the Molpro2020 program.[44] The CCSD(T)-F12a/cc-pVTZ-F12 calculations were performed with the recommended correlation factor of $\beta = 1.0$, the frozen core approximation, and default convergence criteria.[42,43] For the 1D, 2D, and 3D PES cuts, we use the displacement range given in Table S1, with a step size of 5°/0.05 Å, 10°/0.10 Å, and 15°/0.15 Å, respectively. The PES was subsequently evaluated at the respective quadrature points using cubic spline interpolation to reduce the number of single points CCSD(T)-F12a/cc-pVTZ-F12 calculations. In contrast, the **G** matrix elements were not interpolated, but calculated directly at each quadrature point.

B. Coordinates

The structure of the water dimer can be described by 12 curvilinear internal coordinates; chosen to be r_1, r_2, t_{a}, r_3, r_4, t_{d}, R, θ, ϕ, α, β, and γ. The intramolecular coordinates, $\{r_1,\ r_2,\ t_{\text{a}}\}$ and $\{r_3,\ r_4,\ t_{\text{d}}\}$ are the bond

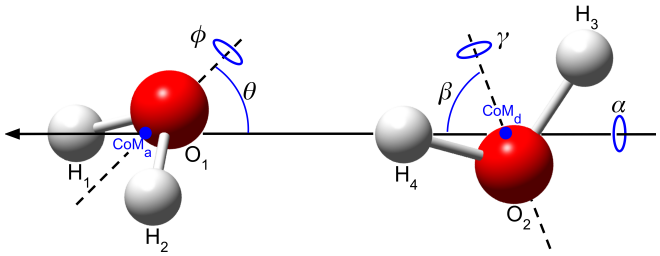

FIG. 1. Definition of the intermolecular internal coordinates of the water dimer and the numbering of the atoms of the two H_2O units.

lengths (r) and the bond angles (t) of the acceptor and donor units, respectively. As seen in Fig. 1, R is the distance between the center of masses (CoMs) of the two units. The intermolecular angles: ϕ and γ describe the rotation of the acceptor and donor around the bisector of their bond angles, respectively, and θ and β denote the angle between these bisectors and the CoM–CoM axis, respectively. The angle α describes the rotation of the two H_2O units relative to each other along the CoM–CoM axis. In Section S2 A of the Supplementary Information (SI), we provide instructions on how Cartesian coordinates are obtained from the internal coordinates. The values of the internal coordinates corresponding to the equilibrium structure for the different PES are shown in Table S7. Since the CoM–CoM distance depends on the masses of the atoms, we note here that the masses $m_{\mathrm{H}} = 1.007\,825$ u and $m_{\mathrm{O}} = 15.994\,915$ u have been used.

C. Symmetry aspects

Molecular symmetry (MS) groups[32] can be employed to describe the true (observable) symmetry of vibrational-rotational-tunneling (VRT) states of molecules. The MS group includes feasible permutations of identical nuclei and the inversion operator. The MS group of the water dimer is G_{16} (isomorphic to the D_{4h}(M) group), which includes permutation of the hydrogens within the monomers, permutation of the donor and acceptor, and the inversion operation.[32,45] In Table I, we show the effect of the generators of G_{16}, and its subgroup G_8 (where the permutation of the donor and acceptor units is excluded), on the internal coordinates. Applying the operators of G_{16} results in 16 different numbering of the nuclei of the water dimer. However, since the equilibrium structure has C_s point-group symmetry (see Fig. 1), there are only eight distinct versions of

TABLE I. Action of the generators[a] of the molecular symmetry groups G_8 and G_{16} on the internal coordinates. See Fig. 1 for the definition of the coordinates.

G_{16}				
G_8				
E	(12)	(34)	E^*	P_{da}
β	β	β	β	$\pi-\theta$
θ	θ	θ	θ	$\pi-\beta$
ϕ	$\phi+\pi$	ϕ	$2\pi-\phi$	$\gamma+\pi$
α	α	α	$-\alpha$	α
γ	γ	$\gamma+\pi$	$2\pi-\gamma$	$\phi+\pi$
r_1	r_2	r_1	r_1	r_3
r_2	r_1	r_2	r_2	r_4
t_{a}	t_{a}	t_{a}	t_{a}	t_{d}
r_3	r_3	r_4	r_3	r_1
r_4	r_4	r_3	r_4	r_2
t_{d}	t_{d}	t_{d}	t_{d}	t_{a}

[a] The generator (12) permutes H_1 and H_2, (34) permutes H_3 and H_4, and $E*$ denotes inversion. The generator $P_{\mathrm{da}} \equiv (O_1O_2)(13)(24)$ permutes the donor and acceptor nuclei.

the equilibrium structure that can be interconverted into each other. These eight versions are separated by relatively small barriers; therefore, tunneling between the different minima is pronounced, causing each vibrational level to split into eight VRT levels. For further details on employing symmetry for the water dimer, see Refs. 32 and 45.

As the VRT states transform according to the irreducible representations of the MS group(s), it is possible to construct the Hamiltonian matrix in a block-diagonal form, where each block corresponds to one irreducible representation of (a subgroup of) the MS group. This facilitates the assignment of the computed states and improves the convergence properties of the diagonalization routine, as the almost degenerate states are treated independently.

To take advantage of permutation-inversion symmetry, the reference structure and the coordinate choice should be compatible with the generators of the group. This means that the 1D eigenfunctions (or their product) corresponding to the 1D Hamiltonian of Eq. (5) should be eigenfunctions of the permutation-inversion operators, as well. Based on this restriction, we use the G_8 MS group[32] to construct the block-diagonal form of the Hamiltonian matrix. For the coordinate definition used in this work, the reference value of OH bond lengths on the donor should be equal as should the OH bond lengths of the

acceptor. We define the reference structure of a given PES from the optimized geometry, where the OH bond lengths of the donor is set to the average of the two OH bond lengths (see Table S7 for reference and optimized structures). In this case, the 1D potential along ϕ is symmetric for $\phi \to \phi + \pi$ and $\phi \to 2\pi - \phi$, and the same is true for γ, and the 1D potential along α is symmetric for $\alpha \to 2\pi - \alpha$. Therefore, the 1D eigenfunctions for ϕ, γ and α are eigenfunctions of the generators ((12), (34) and E^*) of G_8 [see Table I]. For the chosen reference structure, the potential energy surface in the β and θ directions is not symmetric around $\pi/2$. Therefore, the 1D eigenfunctions for β and θ are not eigenfunctions of the P_{da} operator present in G_{16}, and primitive basis functions should be used for these two coordinates in order to utilize G_{16}. As P_{da} interchanges the donor and acceptor units, and in addition to the constraint on the basis functions associated with the β and θ coordinates, both OH-bond lengths and HOH-bond angles of the reference structure should be equivalent to take advantage of G_{16}. To avoid this constraint, we have opted for using the subgroup G_8, rather than G_{16}. Using only G_8 also allows us to use reduced-dimensional models, where the internal coordinates of one monomer is frozen while active for the other monomer.

The generators (12) and (34), in Table I, interchange the OH bond lengths of the acceptor unit and of the donor unit, respectively. The two acceptor OH stretches are equivalent, and we chose their basis functions as the 1D eigenfunctions. The product of the acceptor basis functions are indeed eigenfunctions of the generator (12), if the associated quantum numbers are equivalent

$$(12)\psi_v(r_1)\psi_v(r_2) = \psi_v(r_2)\psi_v(r_1) = 1 \cdot \psi_v(r_1)\psi_v(r_2) \tag{17}$$

The two donor OH stretches are not equivalent. However, the basis functions for both the OH_f stretch and for the OH_b stretch are chosen as the 1D eigenfunctions of the OH_f stretch. With this choice, the product of the donor basis functions become eigenfunctions of the generator (34), if the associated quantum numbers are equivalent.

If the quantum numbers are different ($v \neq v'$), products of the 1D basis functions are not eigenfunctions of the generators:

$$(12)\psi_v(r_1)\psi_{v'}(r_2) = \psi_v(r_2)\psi_{v'}(r_1) \neq \lambda \cdot \psi_v(r_1)\psi_{v'}(r_2) \tag{18}$$

where λ is a constant. There are two apparent solutions to this challenge, either changing the coordinates to symmetric/asymmetric displacements of the OH bond lengths from their equilibrium values, or using a linear combination of the 1D eigenfunctions as basis functions. We have chosen the latter strategy, resulting in basis functions of the type:

$$\psi_{vv'\pm}(r_1, r_2) = \frac{1}{\sqrt{2}} \left(\psi_v(r_1)\psi_{v'}(r_2) \pm \psi_{v'}(r_1)\psi_v(r_2)\right), \tag{19}$$

for both the donor and the acceptor OH stretches. The full (12D) basis functions thus take the following form (with the label of the quantum numbers excluded for ease of notation):

$$\Psi(r_1, r_2, t_{\mathrm{a}}, r_3, r_4, t_{\mathrm{d}}, R, \beta, \theta, \phi, \alpha, \gamma) = \tag{20}$$
$$\psi(r_1, r_2)\psi(t_{\mathrm{a}})\psi(r_3, r_4)\psi(t_{\mathrm{d}})\psi(R)\psi(\beta)\psi(\theta)\psi(\phi)\psi(\alpha)\psi(\gamma).$$

In order to construct the block-diagonal Hamiltonian, we determine the character of each permutation-inversion operator for a given $\Psi(r_1, r_2, t_{\mathrm{a}}, r_3, r_4, t_{\mathrm{d}}, R, \beta, \theta, \phi, \alpha, \gamma)$, and compare the result with the character table of G_8 to determine which irreducible representation the given basis function belongs to.[32] Then, we construct the individual blocks of the Hamiltonian matrix from those basis functions that transform as a given irreducible representation. Using the G_8 MS group results in eight blocks, which significantly reduces the cost of the diagonalization.

D. Polyad truncation & energy ceiling

In VibMEMIC, two strategies are followed to limit the size of the variational basis: a polyad number truncation and an energy ceiling. The polyad truncation is of the type

$$P = \sum_{n}^{M} P_n v_n \leq P_{\max},$$

where v_n is the nth quantum number, P_n is a coefficient, and $P_{\max}$ is the maximum polyad number. For the three vibrations of H_2O, one would typically choose $P_1 = 2$, $P_2 = 1$, and $P_3 = 2$, such that the stretch-bend Fermi resonances are included in the basis, for each value of the quantum numbers included for the OH stretches. Defining effective polyad truncations is crucial in terms of reducing the computational cost of FBR calculations. The maximum polyad number controls the size of the Hamiltonian, but not the relative size of its blocks. For a given value of $P_{\max}$, blocks with basis functions that transform as different irreducible representations can be of different size. The states associated with the largest block will be better converged compared to states associated with smaller blocks. The vibrational tunneling

states of water dimer transform as different irreducible representations. An inappropriate value of $P_{\max}$ can introduce errors in the calculated tunneling splittings, if the magnitude of the tunneling splittings are comparable to the convergence of the energy levels. Hence, we use a polyad truncation for the ϕ and γ modes, to ensure that the different blocks in the Hamiltonian are of similar size.

Setting an energy ceiling is another way to control the size of the basis ($E_{v_1 v_2 ... v_M} \leq E_{\max}$). However, as the $E_{v_1 v_2 ... v_M}$ energy levels are not known *a priori*, the ceiling is typically based on a sum of the 1D energy levels ($E_{v_1 v_2 ... v_M} \approx \sum_n^M E_{v_n}^{\rm 1D} = E_{v_1 v_2 ... v_M}^{\rm approximate} \leq E_{\max}$). Again, care must be taken with respect to resolving tunneling splittings that are comparable to the convergence of the energy levels as $E_{\max}$ also controls the total size of the Hamiltonian, but not the relative size of its blocks. In VibMEMIC both the maximum polyad number and the energy ceiling are chosen to best address the specific problem, and only basis functions that satisfy both truncations are included. In computations with both intramolecular (high-frequency) and intermolecular (low-frequency) modes, polyad truncations and energy ceilings are defined for each set of modes (see Section S1).

E. Notation of transitions

In Section IV, we present intramolecular transitions calculated with different vibrational models. We only give the final state of the transitions as all arise from the ground state. The final state for the intramolecular acceptor transitions are denoted: $|v_i v_j\rangle_{\pm}|v_k\rangle$, where v_i and v_j refer to the OH stretch quanta and v_k refers to the HOH bend quanta. The two OH stretches of the donor are not equivalent and the final states for the intramolecular donor transitions are denoted: $|v_m\rangle_{\rm f}|v_n\rangle_{\rm b}|v_l\rangle$, where v_m and v_n refer to the free (f) and bound (b) OH stretch quanta, respectively, while v_l refers to the HOH bend quanta.

III. FBR VS. DVR

The so-called fourth-age[46] variational nuclear-motion code GENIUSH,[36–38] based on the discrete variable representation (DVR) of the Hamiltonian,[47–52] was employed extensively to benchmark the FBR based VibMEMIC code. The acronym GENIUSH stands for **Ge**neral code with **N**umerical, **I**nternal-coordinate, **U**ser-**S**pecified **H**amiltonians. GENIUSH can be used to solve the time-independent nuclear Schrödinger equation and obtain rovibrational eigenenergies for systems which exhibit several interacting minima. Furthermore, the code allows the straightforward setup of reduced-dimensional models in arbitrary curvilinear internal coordinates. In GENIUSH, both the kinetic and the potential energy operators are treated "exactly", that is, no approximations are introduced. The latest version[38] of the GENIUSH code is capable of treating block-diagonal Hamiltonian matrices, formed according to the irreducible representations of the MS group[32] of the molecule, or at least a subgroup of it.

Although GENIUSH is able to treat rotations,[37] here we only discuss vibrations, for which the Hamiltonian is given in Eq. (1). The basis is the direct product of one-dimensional primitive DVR functions corresponding to each internal coordinate:

$$\psi_{n_1,n_2..,n_M}(q_1,...,q_M) = \prod_{k=1}^{M} \chi_{n_k}(q_k), \qquad (21)$$

where $\chi_{n_k}(q_k)$ is the n_k'th DVR basis function corresponding to the q_k coordinate. If N_1^0, N_2^0,..,N_M^0 primitive DVR functions are used for the first, second, ..., and Mth coordinate, the size of the full direct-product basis is $N^{\rm tot} = \prod_{k=1}^{M} N_k^0$. The $N^{\rm tot} \times N^{\rm tot}$-dimensional matrix of the potential energy becomes diagonal in this basis:

$$V_{(n_1,..,n_M),(n_1',..,n_M')} = V(q_{1,n_1},..,q_{M,n_M}) \prod_{k=1}^{M} \delta_{n_k,n_k'}, \qquad (22)$$

where q_{k,n_k} is the n_kth DVR quadrature (grid) point corresponding to the kth coordinate. The representation of the kinetic energy operator is also an $N^{\rm tot} \times N^{\rm tot}$-dimensional matrix. Therefore, the elements of $\mathbf{G}$ as well as $\tilde{g}$ are evaluated at all the grid points and the matrices of the differential operators are also constructed in DVR. The resulting $N^{\rm tot} \times N^{\rm tot}$-dimensional vibrational Hamiltonian matrix is symmetric and sparse. The required eigenvalues are computed using an iterative Lanczos eigensolver.[53] Table S11 specifies the DVR vibrational basis used in the computations.

To test the accuracy of the FBR based VibMEMIC model, we have performed a set of reduced-dimensional computations with both VibMEMIC and GENIUSH. In Section S3, we show several examples, illustrating that the 1D, 2D, and 3D results with VibMEMIC and GENIUSH generally agree to within ≤ 0.2 cm^{-1}.

The water dimer has eight equivalent versions of its equilibrium structure. These version are sampled, for

TABLE II. Fundamental intramolecular transitions ($\tilde{\nu}$), in cm^{-1}, of the donor (D) and acceptor (A) unit in water dimer separated by 20 Å. The results are obtained with a 3D vibrational model utilizing the MB-pol potential[20] and the DVR-based code GENIUSH.

Final state	Reduction in **g**		Reduction in **G**	
	$\tilde{\nu}$(D)	$\tilde{\nu}$(A)	$\tilde{\nu}$(D)	$\tilde{\nu}$(A)
$\|0\rangle\|0\rangle\|1\rangle$	1586.8	1590.6	1594.4	1594.4
$\|10\rangle_+\|0\rangle$	3656.1	3656.1	3656.1	3656.1
$\|10\rangle_-\|0\rangle$	3741.8	3748.6	3755.0	3755.0

example, in 5D calculations with β, θ, ϕ, α, and γ. However, these eight versions are not equivalent within the many-mode expansion of the PES truncated at third order, which is the approximation utilized in VibMEMIC. As a consequence, the energy levels computed with VibMEMIC appear as two sets of four states, rather than one set of eight states (see Table S3). This symmetry breaking for the many-mode expansion also leads to small non-zero elements in the Hamiltonian connecting the different blocks. We set these small non-zero elements to zero in VibMEMIC, to preserve the block-diagonal structure of the Hamiltonian. From our reduced-dimensional computations we estimate that the difference between enforcing or neglecting this symmetry leads to differences in the intramolecular fundamentals of no more than 0.2 cm^{-1}.

Both the new FBR-based VibMEMIC code and the DVR-based GENIUSH code have advantages and limitations and are optimal for slightly different situations. The size of the Hamiltonian matrix is much smaller in the FBR-based VibMEMIC code than in the DVR-based GENIUSH code, which allows inclusion of more vibrational modes. Furthermore, the efficient truncation of the basis, by the polyad numbers and by the energy ceilings, also helps limit the size of the Hamiltonian matrix within VibMEMIC. Thus, compared to GENIUSH, the diagonalization part of the computation is significantly faster with VibMEMIC.

IV. RESULTS & DISCUSSION

A. The Kinetic Energy in Reduced Dimensions

In reduced-dimensional (ro)vibrational models with M active coordinates, the remaining $3N-M$ coordinates are inactive (constrained), and an effective Hamiltonian that incorporates these constraints must be constructed. The constraints can either be taken into account by removing the rows and columns involving the constrained coordinates in **G**, or by removing the corresponding rows and columns in **g**. The latter option results in a constrained **G** after inversion of **g** [see Eqs. (2) and (3)]. If the coordinates are orthogonal, the two approaches are equivalent. However, if the coordinates are not orthogonal, the two approaches give rise to different effective Hamiltonians and, consequently, different results. In classical mechanics, constraining the coordinates corresponds to $dq_i/dt = 0$, where i is an index of an inactive mode. The **G** matrix obtained from this type of constraints corresponds to removing columns and rows in **g**. In comparison, the reduction in **G** is equivalent to setting $p_i = 0$.

In Table II, we present reduced-dimensional (3D) calculations of the fundamental intramolecular transitions of the two water units in water dimer, where the two monomers have been separated by 20 Å (R = 20 Å). Since the two monomer units are separated by 20 Å, we expect the fundamentals of the donor and the acceptor to be identical. This is indeed the case when **G** is reduced. However, the calculated intramolecular transitions presented in Table II clearly depend on whether the constraints are introduced in **g** or **G**. When **g** is reduced, the intramolecular fundamentals of the two units differ significantly for the bend and the antisymmetric stretch. If **G** is reduced, then the resulting **G** matrix is the same as that of the free water molecule (see Section S2 B). In the 3D computations for the donor or acceptor units, the **G** matrix does not depend on the R, and the 3D kinetic energy operator is the same if R is fixed to its equilibrium value or 20 Å. As shown in Table II, for this particular constrained model, reduction in **g** results in an erroneous description of the intramolecular transitions of the two H_2O units as clearly illustrated in the dissociation limit. Therefore, we employ the reduction in **G** for the rest of the paper.

B. Choice of the intermolecular distance coordinate (O–O vs. CoM–CoM)

For weakly-bound dimers, the coordinates associated with the intermolecular modes are typically defined as five Euler angles and one distance, describing the relative orientation and distance between the donor and acceptor units, respectively. The donor-acceptor distance coordinate is typically defined from the CoMs of the two units, for which an analytical expression for the kinetic

energy operator has been derived.[54] In both GENIUSH and VibMEMIC, the kinetic energy operator is represented numerically, which facilitates the exploration of alternative coordinate definitions. One alternative intermolecular distance coordinate in the case of the water dimer is the O–O distance, which is often the distance coordinate of choice if one defines the coordinates from a Z matrix. The CoM-CoM definition is general for bimolecular complexes, but unlike the O–O definition, it is not isotopically invariant.

In terms of calculating the intramolecular fundamentals accurately, we define the optimal coordinate as the one which has the least impact on these transitions; thus, likely requiring fewer basis functions to converge the intramolecular fundamentals. In Table III, we show the wavenumber shift of the intramolecular fundamentals calculated from a (3+1)D and a 3D calculation of the donor and acceptor intramolecular modes. The 3D in (3+1)D represents the donor or acceptor intermolecular modes and the '+1D' refers to adding the intermolecular mode associated with the distance coordinate. In other words, a 4D calculations without an adiabatic separation. The inactive coordinates were fixed to their reference value. As seen in Table III, the CoM–CoM coordinate choice has significantly smaller impact on the intramolecular fundamentals than the O–O choice. Therefore, we employ the CoM–CoM coordinate in all computations.

C. Interunit coupling

For most practical purposes the coupling between the intramolecular modes of the donor and acceptor units is expected to be negligible. The addition of such coupling terms to a harmonically-coupled anharmonic-oscillator model resulted in transition wavenumber changes of $\sim$1 cm^{-1}.[55] In Table IV, we compare selected intramolecular transition wavenumbers calculated with a 3D model for the three intramolecular modes of either the donor or acceptor, with those calculated with a 6D model that includes all intramolecular modes simultaneously. As seen in Table IV, the computed intramolecular transition wavenumbers with (6D) and without (3D) interunit coupling (IUC) do not deviate more than 2.5 cm^{-1}. These transition wavenumber changes are small compared to the shifts induced by the intermolecular modes (*vide infra*). In the forthcoming sections we focus on the coupling of either the donor or the acceptor intramolecular modes with the intermolecular modes, with the approximation that the interunit coupling can be neglected.

TABLE III. Wavenumber differences ($\Delta\tilde{\nu}$, in cm^{-1}) of the intramolecular fundamentals with and without including the R mode. Two different definitions of the donor-acceptor distance coordinate are used. Results are shown for both the donor, (D), and acceptor, (A), unit. The results are obtained with the MB-pol PES[20] using GENIUSH.

Final state	CoM–CoM		O–O	
	$\Delta\tilde{\nu}$(D)	$\Delta\tilde{\nu}$(A)	$\Delta\tilde{\nu}$(D)	$\Delta\tilde{\nu}$(A)
$\|0\rangle_f\|0\rangle_b\|1\rangle$ or $\|00\rangle\|1\rangle$	−0.38	0.07	−1.21	0.72
$\|0\rangle_f\|1\rangle_b\|0\rangle$ or $\|10\rangle_+\|0\rangle$	−0.10	0.01	1.21	−0.10
$\|1\rangle_f\|0\rangle_b\|0\rangle$ or $\|10\rangle_-\|0\rangle$	3.41	0.28	−4.63	0.31

TABLE IV. Calculated transition wavenumbers, in cm^{-1}, for selected OH stretch and HOH bend transitions in the water dimer. Results from a 3D model for either the donor or the acceptor modes is compared with results from 6D model that includes all six intramolecular modes. The results are obtained using VibMEMIC and the F12 PES.

Final state	3D	6D	$\Delta\tilde{\nu}$
$\|00\rangle\|1\rangle$	1596.7	1595.2	−1.5
$\|0\rangle_f\|0\rangle_b\|1\rangle$	1614.2	1614.5	0.3
$\|00\rangle\|2\rangle$	3157.1	3155.1	−2.0
$\|0\rangle_f\|0\rangle_b\|2\rangle$	3191.1	3188.7	−2.4
$\|0\rangle_f\|1\rangle_b\|0\rangle$	3558.0	3555.5	−2.5
$\|10\rangle_+\|0\rangle$	3651.7	3651.6	−0.1
$\|1\rangle_f\|0\rangle_b\|0\rangle$	3726.9	3726.9	0.0
$\|10\rangle_-\|0\rangle$	3746.6	3746.0	−0.6

D. Coupling between intramolecular and intermolecular modes

In spectra of hydrogen-bonded complexes, the bound XH-stretch fundamental (where X is an electronegative donor atom, for example, O) is often detected, as it typically becomes redshifted and its intensity is enhanced relative to the corresponding transition of the isolated monomer.[56,57] For complexes with water as the donor unit, the two OH stretches become partly decoupled upon complex formation, due to the frequency shift associated with hydrogen-bond formation. The bonded OH stretch, OH_b, is redshifted relative to both OH stretches of the monomer, because the hydrogen bond weakens the OH_b bond. The free OH stretch, OH_f, is redshifted relative to the antisymmetric fundamental of the water monomer, as the coupling between the two OH stretches is reduced.

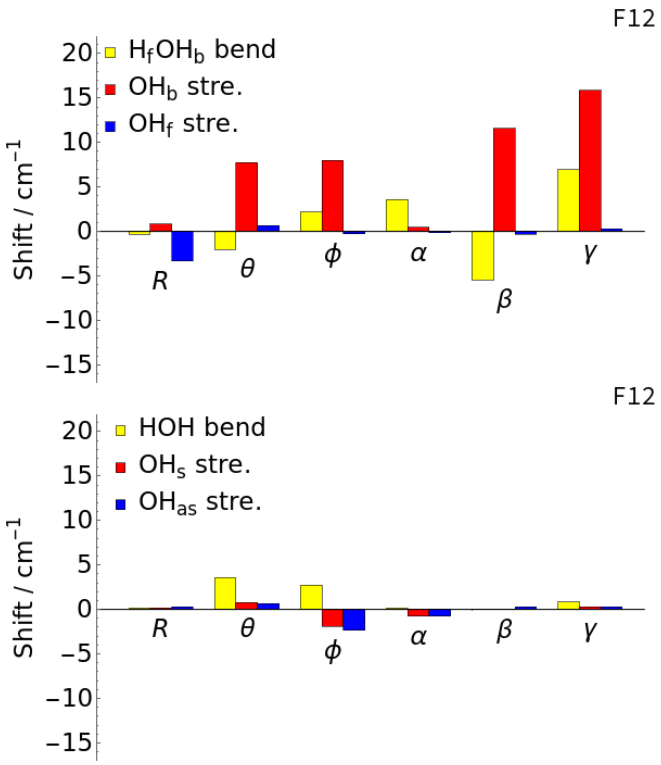

FIG. 2. Shifts of the donor (upper panel) and acceptor (lower panel) transitions, due to coupling one intermolecular mode (resulting in (3+1)D models) to the donor or acceptor intramolecular modes (3D model). The results were obtained using the F12 PES with VibMEMIC.

In contrast, the bending transitions of the donor unit are blueshifted, because the hydrogen bond "locks" H_b, which hinders the bending motion.

In order to investigate the effect of the individual intermolecular modes on the OH stretch and HOH bend transitions, we performed a series of (3+1)D computations, where the three modes of either the donor or the acceptor unit and one of the intermolecular modes were active. In these computations symmetry was not utilized. In Figure 2, we show the shifts of the donor and acceptor fundamentals, based on the (3+1)D computations relative to 3D computations. The shifts presented in Fig. 2 are obtained with the F12 PES with VibMEMIC, while the results calculated with GENIUSH for the MB-pol and CCpol PESs are given in Section IV E. Overall, the shifts are similar to previous results obtained with a simplified effective Hamiltonian approach with a similar coordinate system as the one employed here.[22]

For the donor unit, the calculated shifts for the free OH (OH_f) stretch are small, as this oscillator is not directly involved in hydrogen bonding. The shifts induced by coupling to the intermolecular modes can be traced back to either potential or kinetic energy coupling. The small shifts associated with this mode reflect not only that the potential energy coupling with the intermolecular coordinates is small, but also that the **G** matrix elements of the intermolecular modes depend only weakly on the OH bond lengths. The shift of the OH_b stretch is positive for all coordinates, it is largest for β and γ. Coupling of β or γ to the donor vibrations enables partially breaking the hydrogen bond;[22,24] thus, significantly blueshifting the OH_b stretch with respect to the 3D values. A positive displacement of the R coordinate increases the CoM–CoM distance, partially breaking the hydrogen bond, but negative displacements along this coordinate have the reverse effect. For water dimer, the net effect of including R is small, in agreement with what has been found in previous studies.[22,58] For the donor bending fundamental, we observe negative shifts for θ and β, and positive shifts for the other angle coordinates, but practically zero shift for R.

Potential energy coupling is evident when 1D PES cuts along the OH_b (r_4) or the bending (t_d) coordinates, depend on the value of the intermolecular coordinates. Kinetic energy coupling is mostly caused by the dependence of G_{ii} (for the intermolecular angles) on the value of the bond lengths and bond angle. The $G_{r_4r_4}$ and $G_{t_dt_d}$ elements do not depend on the intermolecular angles and the off-diagonal elements of the **G** matrix have minuscule effect on the vibrations of the donor unit. Cuts of the PES along r_4 and t_d, corresponding to different values of the intermolecular angles, are shown in Figs. S1 and S2. The G_{ii} element for $i = \alpha, \beta, \gamma$, as a function of i and r_4 or t_d, are shown in Fig. S4. In addition, (3+1)D computations where all two- and three-mode terms involving the intermolecular mode were excluded from the PES, were used to "turn off" the potential energy coupling (see Table S13). If the results from such computation are similar to the 3D results, then the potential energy coupling is responsible for the shift, while if it is similar to the original (3+1)D results, then the shift is due to kinetic energy coupling.

In the case of θ and ϕ, the shifts of the donor bend and the OH_b stretch modes are due fully to potential energy coupling between the inter- and intramolecular coordinates, since the **G** matrix elements involving θ and ϕ do not depend on the donor's intramolecular coordinates, and *vice versa*. This was also confirmed by the fact that we retrieved the 3D results when we turned off the potential energy coupling in the (3+1)D calculations. In addition, the PES along r_4 or t_d depends on the

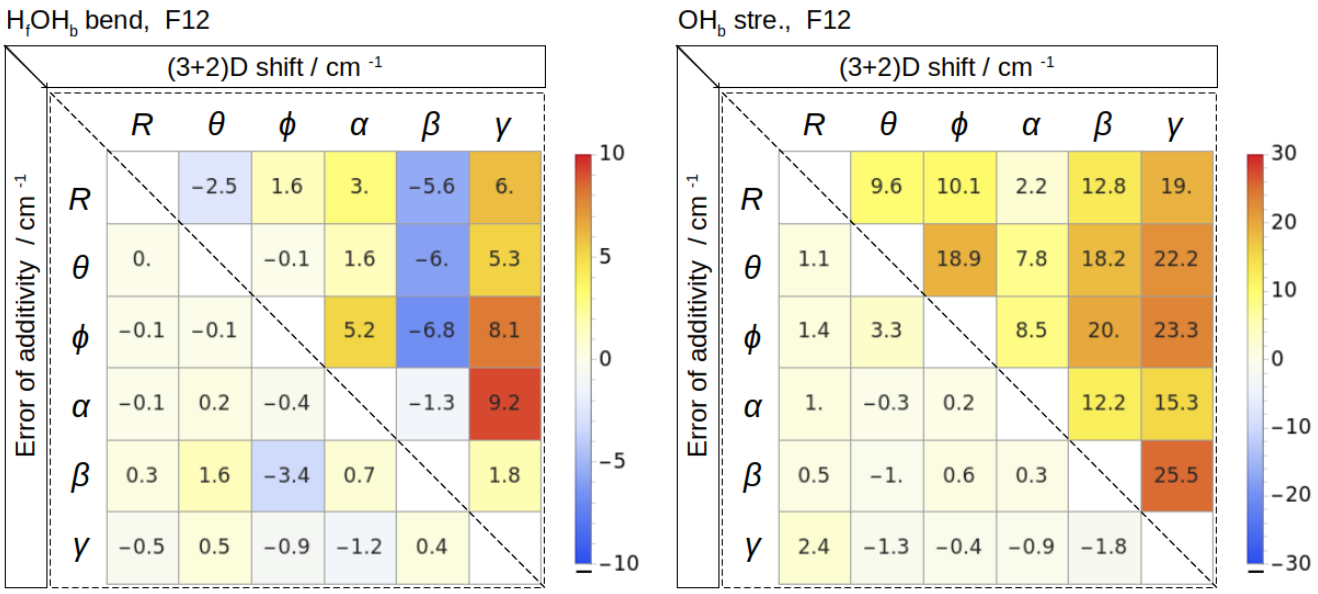

FIG. 3. Shifts of the bend and OH_b stretch donor vibrations obtained by coupling two intermolecular modes to the three donor modes ((3+2)D model). The error of additivity is the difference of the (3+2)D shifts and two (3+1)D shifts that involve the two intermolecular modes that are in the (3+2)D model. Note the significant difference in the color scale. The results were obtained using the F12 PES with VibMEMIC.

value of θ and ϕ chosen for the cut and this dependence mostly explains the direction of the shift. For example, the potential along r_4 becomes steeper if ϕ is not at its equilibrium value and activating the ϕ coordinate means that these non-equilibrium values are sampled; therefore, the OH_b fundamental transition wavenumber increases.

In the case of α, β, and γ, both the potential and the kinetic energy coupling may affect the frequency of the donor bend and the OH_b stretch modes. The shift of the donor bend induced by α and γ is caused mainly by kinetic energy coupling, since the PES along t_d only slightly depends on α and γ. In contrast, $G_{\alpha\alpha}$ and $G_{\gamma\gamma}$ strongly depend on t_d. The redshift of the bending due to β can be traced to potential energy coupling. This is evident from the (3+1)D calculations with the potential energy coupling turned off. The PES along t_d becomes less steep if β is not at its equilibrium value, and $G_{\beta\beta}$ depends only slightly on t_d. The shift of OH_b due to β and γ involves both kinetic and potential energy coupling. In the case of β and γ, the potential energy coupling causes a large positive shift (in agreement with the 1D PES cuts), while the kinetic energy coupling causes a small negative shift in the case of β. The kinetic energy coupling between γ and the donor turned out to be very sensitive to the OH bond lengths and consequently, the induced shifts depend on the average bond length which depend on the PES. For example, in the case of the MB-pol PES, kinetic energy coupling for γ induces -3.9 and -0.5 cm^{-1} shifts in the OH_b and OH_f transition wavenumbers, respectively, while the shifts are 1.2 and -1.9 cm^{-1} for the F12 PES.

For the acceptor unit, the wavenumber differences from the (3+1)D computations and the 3D computation are shown in the lower panel of Fig. 2. The intramolecular fundamentals of the acceptor unit are not strongly affected by complex formation and are similar to those of an isolated water molecule. The shifts seen for the fundamentals of the acceptor unit are indeed much smaller than those seen for the donor unit in the upper panel of Fig. 2. The largest corrections to the bending transition are seen for θ and ϕ, the two intermolecular modes directly associated with the acceptor unit. By performing calculations with only kinetic energy or potential energy coupling between the intra- and intermolecular modes, we traced the majority of effect to a single term in the kinetic energy operator for each intermolecular mode. The diagonal $\mathbf{G}$ matrix elements for θ and ϕ, $G_{\theta\theta}$ and $G_{\phi\phi}$, respectively, both depend strongly on the HOH bending angle of the acceptor unit. This dependence is far from linear and the vibrationally averaged kinetic energy of these intermolecular modes are thus different for the HOH-bending ground and excited states, resulting in the observed wavenumber corrections seen in the lower panel of Fig. 2 for the acceptor bending transition.

To investigate if the shifts from each of the intermolecular modes are additive, we performed 15 sets of (3+2)D model calculations. The "+2D" means adding a pair of intermolecular modes to the 3D model of the intramolecular modes, resulting in a 5D calculation. The shifts calculated with 15 different (3+2)D models for the OH_b stretch and HOH bend fundamental of the donor unit are shown in the upper triangles of the two panels of Fig. 3. In the lower triangles of Fig. 3, we show the shifts computed for the (3+2)D models minus the shifts calculated for the related two (3+1)D models. The upper triangles thus display the total shifts calculated with different (3+2)D models, while the lower triangles reflect the degree to which the shifts are additive.

For the donor HOH bend fundamental, the (3+2)D shifts for pairs involving γ are positive, while negative values occur for pairs involving β. This correlates with the (3+1)D results for γ or β (Fig. 2). The largest discrepancies in the additivity of the (3+1)D shifts for the bending are observed for the (θ,β) and (ϕ,β) pairs (1.6 and -3.4 cm^{-1} error in the -6.0 and -6.8 cm^{-1} (3+2)D shifts, respectively). For the bound OH stretch fundamental, the largest discrepancy is found for the (θ,ϕ) pair, with a 3.3 cm^{-1} error in the 18.9 cm^{-1} shift. For most pairs, the (3+2)D corrections are approximated well by the sum of two (3+1)D shifts.

We attribute the partial breakdown of the additivity of the shifts for the bend, but not for the bound OH stretch, to the difference in the nature of the coupling to the intermolecular modes. The PES along the bound OH-stretching coordinate changes significantly upon varying the value of some of the intermolecular coordinates. The intermolecular modes predominantly affect the bound OH stretch due to vibrationally averaging effects, and not through resonances between states with excitations in both the bound OH stretch and the intermolecular modes. In contrast, analogous resonances do play an important role for the bending states. The strength of a resonance depends on the size of the coupling element and the energy difference between the states involved in the resonance. When two intermolecular modes are included simultaneously, the two intermolecular modes couple, thus altering the energy levels associated with each intermolecular mode and hence the strength of the resonance(s) - leading to a partial breakdown of the additivity of the shifts for the bend.

In general, the additivity of the calculated shifts works well, which indicates that the total shift induced by all intermolecular modes can be approximated by the sum of the six (3+1)D shifts. The error of this approximation can be estimated by the size of the errors in the additivity found from the (3+2)D calculations. The advantage of replacing a 9D calculation, including three intramolecular and six intermolecular modes, with six 4D calculations is obvious.

TABLE V. Transition wavenumbers, in cm^{-1}, for selected intramolecular transitions calculated for different PESs, based either on 3D calculations or including the sum of the six calculated (3+1)D shifts, (3+$\sum$1)D.

Final state	3D			(3+$\sum$1)D		
	F12	MB-pol	CCpol	F12	MB-pol	CCpol
$\|00\rangle\|1\rangle$	1596.7	1594.4	1597.1	1603.8	1600.6	1601.5
$\|0\rangle_f\|0\rangle_b\|1\rangle$	1614.2	1607.9	1608.8	1618.7	1614.2	1613.3
$\|00\rangle\|2\rangle$	3157.1	3150.9	3157.3	3172.6	3165.2	3167.6
$\|0\rangle_f\|0\rangle_b\|2\rangle$	3191.1	3177.5	3180.6	3197.7	3188.5	3189.6
$\|0\rangle_f\|1\rangle_b\|0\rangle$	3558.0	3553.6	3543.3	3602.1	3598.5	3585.0
$\|10\rangle_+\|0\rangle$	3651.7	3654.4	3657.3	3649.9	3649.7	3647.5
$\|1\rangle_f\|0\rangle_b\|0\rangle$	3726.9	3728.4	3738.0	3723.4	3731.4	3734.0
$\|10\rangle_-\|0\rangle$	3746.6	3745.9	3750.7	3744.6	3743.8	3738.9

E. Comparison of potential energy surfaces

We have used three different PESs: CCSD(T)-F12a/cc-pVTZ-F12 (abbreviated as F12), CCpol-8sfIR,[19,23] version from the SI of Ref. 23 (abbreviated as CCpol), and MB-pol.[20] In Table V, we show the OH stretch and HOH bend transition wavenumbers from 3D calculations and from 3D including the sum of the shifts from the six (3+1)D computations [the (3+$\sum$1)D model]. We observe that the 3D wavenumbers of the stretching transitions are similar for the F12 and the MB-pol PESs, while the CCpol results are different. For example, the OH_b stretch fundamental obtained with the CCpol PES is about 15 cm^{-1} lower than the F12 and MB-pol values, while the OH_f stretch fundamentals are higher by the same amount. The three PES also give rise to considerable differences for the donor bend, where there is a ~ 6 cm^{-1} difference between the F12 and MB-pol values for the fundamental transition.

In Figs. 4 and 5, we show (3+1)D shifts computed with the different PES for the donor and acceptor OH stretch and HOH bend transitions, respectively. The F12 and the MB-pol PES give very similar (3+1)D shifts, the most noticeable difference is the difference in sign of the shift of the OH_f wavenumber due to R. The difference in

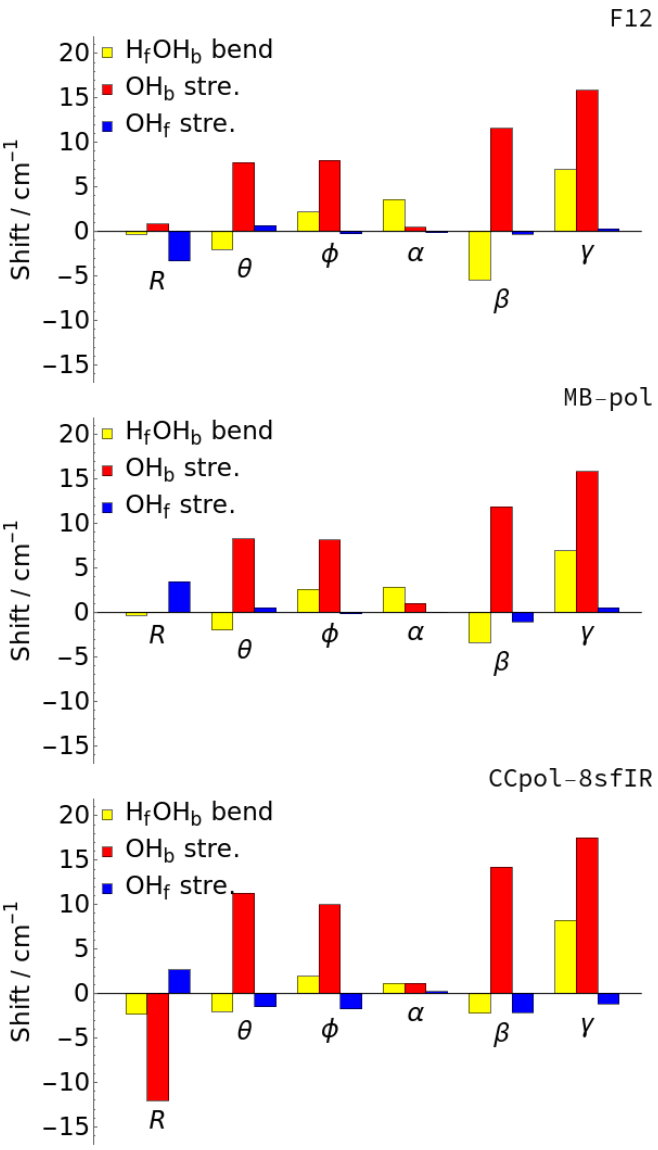

FIG. 4. Upper panel: F12 PES, VibMEMIC. Middle panel: MB-pol, GENIUSH. Lower panel: CCpol-8fsIR PES, GENIUSH. Shift of the donor vibration energies due to coupling one intermolecular moe ((3+1)D model) to the intramolecular modes of the donor (3D model). Please note the different scale with respect to Fig. 5.

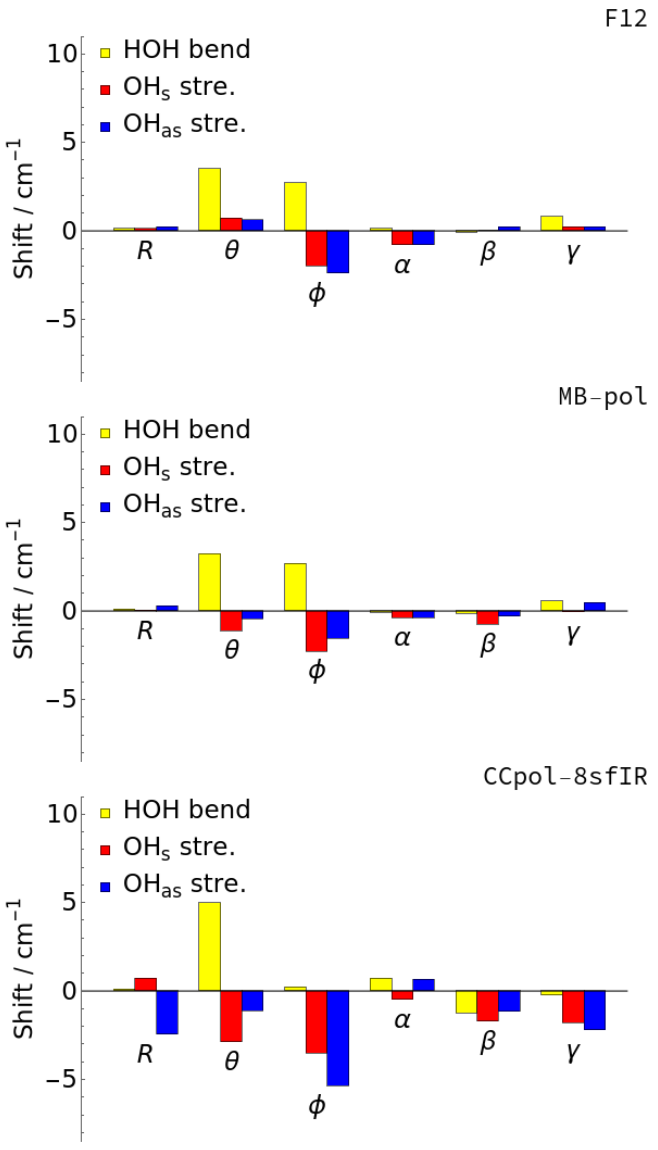

FIG. 5. Upper panel: F12 PES, VibMEMIC. Middle panel: MB-pol PES, GENIUSH. Lower panel: CCpol-8fsIR PES, GENIUSH. Shift of the acceptor vibration energies due to coupling one intermolecular moe ((3+1)D model) to the internal coordinates of the donor (3D model). Please note the different scale with respect to Fig. 4.

sign gives rise to the increase in the difference of the OH_f wavenumbers computed with MB-pol and F12 PES, from 1.5 cm^{-1} in the 3D model, to 8.0 cm^{-1} in the (3+$\sum$1)D model.

The most significant difference between the results with CCpol and the two other PES is the large negative shift of −12.1 cm^{-1} for OH_b, due to R. The OH_b shifts calculated with CCpol are slightly larger for the other intermolecular modes. For the F12 and MB-pol PES, the 1D cuts along OH_b (see Figs. S2 and S3) become less steep if R is decreased and steeper if R is increased. The magnitude of the change is similar for positive and negative displacements of R from the reference value. Furthermore, the 1D ground state wave function for R can to a first approximation be treated as being symmetric with respect to positive and negative displacements, which explains the close to zero total shift of OH_b. For the CCpol PES, the 1D cuts along OH_b are similar to those obtained with the other two PES for increasing R, but become much less steep for negative

displacements of R, thus explaining the large redshift of OH_b due to R seen in Figure 4. Interestingly, for the OH_b fundamental transition, the large redshift due to R is partly compensated by the increased blueshift for the other modes in the (3+$\sum$1)D model, and the difference between the F12 and the CCpol values is quite similar in the 3D model and the (3+$\sum$1)D model (Table V). However, for the CCpol PES the resulting OH_b fundamental in the (3+$\sum$1)D model is 16 cm^{-1} less than the experimental value of 3601 cm^{-1} (*vide infra*), while the agreement with experiment is better than 2 cm^{-1} for the two other PES. This suggests that the coupling of OH_b with R is overestimated in the CCpol PES, which is partly compensated by the overestimation of the coupling with the other coordinates. For the CCpol PES, we find from the (3+2)D donor computations that the additivity of the (3+1)D shifts breaks down if one of the coordinates is R, while there are no problems for F12 and MB-pol. This again suggests that the coupling with R may not be perfectly described in the CCpol PES.

The calculated (3+1)D shifts of the acceptor vibrations are also different for the CCpol PES and the two other PES. The redshifts of the symmetric and antisymmetric stretches are larger in the case of the CCpol PES. Overall, the results for the F12 surface and the MB-pol PES are very similar for these reduced-dimensional computations, but the CCpol PES gives somewhat different results.

F. Reduced- vs. full-dimensional models

In Table VI, observed and computed wavenumbers are presented for selected OH stretch and HOH bend intramolecular transitions. The observed values are obtained from different jet-expansion experiments.[59–64] The computed values are obtained with different reduced-dimensional vibrational models and with a full 12D vibrational model using VibMEMIC and the F12 PES.

As seen in Table VI, the wavenumbers computed with the 3D model are already within about 6 cm^{-1} of the observed values, for five of the six fundamentals. The exception is the bound OH-stretch, which is the mode most affected by dimer formation and, as a consequence, also by the intermolecular modes.[22,56] For the bound OH stretch fundamental, the shifts induced by the intermolecular modes were found to be largely additive (see Section IV D). Based on the additivity analysis, it is not surprising that the (3+$\sum$1)D model significantly improve the OH_b fundamental transition wavenumber. The 3D calculated OH_b fundamental transition wavenumber is 43 cm^{-1} from the observed value, but improves to within ∼1 cm^{-1} of the observed value with the (3+$\sum$1)D model.

For the other intramolecular fundamentals, the calculated differences from the 3D to (3+$\sum$1)D results is less than 7 cm^{-1}, and the agreement with the experimental values remain good. The interunit coupling is small (Section IV C), and adding the calculated corrections to the (3+$\sum$1)D results slightly improves the agreement of the two bending fundamental transitions and has little impact on the stretching transitions.

The transition wavenumbers calculated with the 9D models, where we include the three intramolecular modes of one H_2O unit and all six intermolecular modes, are similar to those computed with the computationally inexpensive (3+$\sum$1)D model. The (3+$\sum$1)D and 9D results are within 2 cm^{-1}.

The transition wavenumbers calculated with the 12D model are similar to the results calculated with the 9D and (3+$\sum$1)D models. The error arising from the inaccuracy of the electronic structure method is expected to be about 5 cm^{-1} with CCSD(T)-F12a/cc-pVTZ-F12.[65–67] The estimated convergence error of the 12D calculations is less than 2 cm^{-1} (Table S6). All models give results in excellent agreement with the experimentally observed transitions from jet expansion experiments. The largest difference between the 12D vibrational calculations and the observed values is seen for the OH_f stretch fundamental transition, i.e., also the transition with the largest difference in the (3+1)D shifts computed with the MB-pol PES and the F12 PES (Section IV E).

Even in recent years, the assignment of the OH_b stretch fundamental transition in water dimer has been debated.[34] In jet expansion experiments, both dimers and high-order (trimer, tetrameter, etc.) clusters often contribute to the observed spectra. In our 3D calculations, the OH_b stretch fundamental transition is located at 3558 cm^{-1}, which happens to be close to the observed OH_b stretch fundamental transition of the water trimer. However, including the coupling to the intermolecular modes, the OH_b stretch transition of the water dimer blueshifts to about 3600 cm^{-1} as seen from the (3+$\sum$1)D, the 9D and the 12D models. The agreement of these vibrational models suggest that the 12D values are reliable, and the calculated OH_b fundamental transition is indeed in excellent agreement with the transition observed at 3601 cm^{-1}.[60]

TABLE VI. Transition wavenumbers, in cm^{-1}, for selected intramolecular transitions of the two water units in water dimer calculated with different vibrational models. The calculated results were obtained using the F12 PES with VibMEMIC. The convergence of the 9D and 12D results are shown in Section S1.

Final state	3D	(3+$\sum$1)D	(3+$\sum$1)D+IUC	9D	9D+IUC	12D	Jet
$\|00\rangle\|1\rangle$	1596.7	1603.8	1602.3	1605.8	1604.3	1605.5	1600.6[61]
$\|0\rangle_f\|0\rangle_b\|1\rangle$	1614.2	1618.7	1619.0	1616.6	1616.9	1616.7	1620[61]
$\|00\rangle\|2\rangle$	3157.1	3172.6	3170.6	3178.0	3176.0	3177.2	#
$\|0\rangle_f\|0\rangle_b\|2\rangle$	3191.1	3197.7	3195.3	3194.9	3192.5	3198.8	#
$\|0\rangle_f\|1\rangle_b\|0\rangle$	3558.0	3602.1	3599.6	3600.0	3597.5	3597.5	3601[60]
$\|10\rangle_+\|0\rangle$	3651.7	3649.9	3649.8	3648.1	3648.0	3648.2	3651[64]
$\|1\rangle_f\|0\rangle_b\|0\rangle$	3726.9	3723.4	3723.4	3721.9	3721.9	3723.0	3730[59]
$\|10\rangle_-\|0\rangle$	3746.6	3744.6	3744.0	3744.2	3743.6	3740.7	3745.5[59]

V. CONCLUSIONS

A new vibrational model and an associated computer code have been developed. The model is based on the finite-basis representation (FBR) of a Hamiltonian expressed in internal coordinates and employes a low-order many-mode expansion of both the kinetic energy operator and the potential energy surface (PES). The truncations are needed to make the computations on many-mode systems feasible. We use polyad truncations and energy ceilings to control the size of the variational basis. In addition, permutation-inversion symmetry is used to obtain a block-diagonal Hamiltonian, further reducing the cost of the computations. The FBR-based VibMEMIC code developed is applicable to all molecular systems described with either user-defined internal coordinates or internal coordinates based on a Z matrix. While the code is general in this sense, the polyad truncation, the energy ceiling, and the use of symmetry needs to be manually defined for the system of interest.

The VibMEMIC results were benchmarked against a nuclear-motion code, GENIUSH, which does not involve simplification in neither the kinetic energy nor the PES operators. For the OH stretch and HOH bend transitions in water dimer, we find that the errors resulting from truncations in the VibMEMIC model appear to be less than the intrinsic inaccuracy of the PESs employed. The truncation of the many-mode expansion of the PES leads to a breakdown of the permutation-inversion symmetry (G_8) of the Hamiltonian, which primarily affects the tunneling-splitting pattern. Most importantly, the approximations applied in VibMEMIC significantly reduce its computational cost when compared with more exact vibrational models and, as illustrated, facilitate computations with the full 12 vibrational modes of water dimer.

We have performed a set of computationally inexpensive reduced-dimensional computations with both the FBR and DVR based models, to understand the applicability of reduced-dimensional effective Hamiltonian approaches. These were designed to investigate how the high-frequency intramolecular transitions are affected by their coupling to the low-frequency intermolecular modes. Not surprisingly, the effects are largest for the OH stretch directly involved in the hydrogen bond. For this mode, the wavenumber shifts from each of the six intermolecular modes were found to be largely additive. The difference between the calculated and experimental transition wavenumber for the bound OH stretch fundamental is improved from $\sim$43 cm^{-1} in the 3D calculations to only $\sim$1 cm^{-1} upon combining the shifts obtained from six (3+1)D calculations. The same reduced-dimensional models provide valuable physical insight into the origin of the observable shifts, which may be used to predict intramolecular transition wavenumbers of related molecules and to guide the construction of effective vibrational models.

The 12D results, augmented with the additivity analysis, indicate that the excellent agreement between the experimentally observed and the computed transitions is not due to error cancellation. We show that this excellent agreement can be achieved even with the use of reduced-dimensional vibrational models. The accurate calculations of intramolecular transition wavenumber is the first step in obtaining reliable calculated water dimer vibrational spectra.

DATA AVAILABILITY

The data that support the findings of this study are available within the article and its supplementary material. The CCSD(T)-F12a/cc-pVTZ-F12 potential energy surface is available online at: `https://erda.ku.dk/archives/58d1c61242c063781b7161c78f0d94e0/published-archive.html`

ACKNOWLEDGEMENTS

We are grateful for funding from NKFIH (grant no. K138233), the Independent Research Fund Denmark (Grant No. 9040-00142B), the Novo Nordisk Foundation Interdisciplinary Synergy Program grant no. NNF19OC0057374 and computer time from the High Performance Center at the Faculty of Science at the University of Copenhagen. IS was supported by a grant from the ÚNKP-21-3 New National Excellence Programs of the Ministry for Innovation and Technology, supported by the National Research, Development and Innovation Fund.

[1] M. Van Thiel, E. D. Becker, and G. C. Pimentel. Infrared studies of hydrogen bonding of water by the matrix isolation technique. *J. Chem. Phys.*, 27:486–490, 1957.

[2] T. R. Dyke, K. M. Mack, and J. S. Muenter. The structure of water dimer from molecular beam electric resonance spectroscopy. *J. Chem. Phys.*, 66:498–510, 1977.

[3] L. B. Braly, J. D. Cruzan, K. Liu, R. S. Fellers, and R. J. Saykally. Terahertz laser spectroscopy of the water dimer intermolecular vibrations. I. $(D_2O)_2$. *J. Chem. Phys.*, 112:10293–10313, 2000.

[4] S. Kassi, P. Macko, O. Naumenko, and A. Campargue. The absorption spectrum of water near 750 nm by CW-CRDS: contribution to the search of water dimer absorption. *Phys. Chem. Chem. Phys.*, 7:2460–2467, 2005.

[5] T. Kumagai, M. Kaizu, S. Hatta, H. Okuyama, T. Aruga, I. Hamada, and Y. Morikawa. Direct observation of hydrogen-bond exchange within a single water dimer. *Phys. Rev. Lett.*, 100:166101, 2008.

[6] M. Yu. Tretyakov, E. A. Serov, M. A. Koshelev, V. V. Parshin, and A. F. Krupnov. Water dimer rotationally resolved millimeter-wave spectrum observation at room temperature. *Phys. Rev. Lett.*, 110:093001, 2013.

[7] E. A. Serov, M. A. Koshelev, T. A. Odintsova, V. V. Parshin, and M. Yu. Tretyakov. Rotationally resolved water dimer spectra in atmospheric air and pure water vapour in the 188–258 GHz range. *Phys. Chem. Chem. Phys.*, 16:26221–26233, 2014.

[8] A. Mukhopadhyay, W. T.S. Cole, and R. J. Saykally. The water dimer I: Experimental characterization. *Chem. Phys. Lett.*, 633:13–26, 2015.

[9] R. Schwan, C. Qu, D. Mani, N. Pal, L. Meer, B. Redlich, C. Leforestier, J. M. Bowman, G. Schwaab, and M. Havenith. Observation of the low-frequency spectrum of the water dimer as a sensitive test of the water dimer potential and dipole moment surfaces. *Angew. Chem. Int. Ed.*, 58:13119–13126, 2019.

[10] K. Morokuma and L. Pedersen. Molecular-orbital studies of hydrogen bonds. An ab initio calculation for dimeric H_2O. *J. Chem. Phys.*, 48:3275, 1967.

[11] D. F. Coker and R. O. Watts. Structure and vibrational spectroscopy of the water dimer using quantum simulation. *J. Phys. Chem.*, 91:2513–2518, 1987.

[12] N. Goldman, R. S. Fellers, M. G. Brown, L. B. Braly, C. J. Keoshian, C. Leforestier, and R. J. Saykally. Spectroscopic determination of the water dimer intermolecular potential-energy surface. *J. Chem. Phys.*, 116:10148–10163, 2002.

[13] D. P. Schofield and H. G. Kjaergaard. Calculated OH-stretching and HOH-bending vibrational transitions in the water dimer. *Phys. Chem. Chem. Phys.*, 5:3100–3105, 2003.

[14] Y. Scribano, N. Goldman, R. J. Saykally, and C. Leforestier. Water dimers in the atmosphere III: Equilibrium constant from a flexible potential. *J. Phys. Chem. A*, 110:5411–5419, 2006.

[15] D. P. Schofield, J. R. Lane, and H. G. Kjaergaard. Hydrogen bonded OH-stretching vibration in the water dimer. *J. Phys. Chem. A*, 111:567–572, 2007.

[16] X. Huang, B. J. Braams, J. M. Bowman, R. E. A. Kelly, J. Tennyson, G. C. Groenenboom, and A. van der Avoird. New *ab initio* potential energy surface and the vibration-rotation-tunneling levels of $(H_2O)_2$ and $(D_2O)_2$. *J. Chem. Phys.*, 128:034312, 2008.

[17] A. Shank, Y. Wang, A. Kaledin, B. J. Braams, and J. M. Bowman. Accurate ab initio and "hybrid" potential energy surfaces, intramolecular vibrational energies, and classical IR spectrum of the water dimer. *J. Chem. Phys.*, 130:144314, 2009.

[18] Y. Wang, X. Huang, B. C. Shepler, B. J. Braams, and J. M. Bowman. Flexible, *ab initio* potential, and dipole moment surfaces for water. I. Tests and applications for clusters up to the 22-mer. *J. Chem. Phys.*, 134:094509, 2011.

[19] C. Leforestier, K. Szalewicz, and A. van der Avoird. Spectra of water dimer from a new *ab initio* potential with flexible monomers. *J. Chem. Phys.*, 137:014305, 2012.

[20] V. Babin, C. Leforestier, and F. Paesani. Development of a "first principles" water potential with flexible monomers: Dimer potential energy surface, VRT spectrum, and second virial coefficient. *J. Chem. Theor. Comput.*, 9:5395–5403, 2013.

[21] J. C. Howard, J. L. Gray, A. J. Hardwick, L. T. Nguyen, and G. S. Tschumper. Getting down to the fundamentals of hydrogen bonding: Anharmonic vibrational frequencies of $(HF)_2$ and $(H_2O)_2$ from ab initio electronic structure computations. *J. Chem. Theor. Comput.*, 10:5426–5435, 2014.

[22] K. Mackeprang, H. G. Kjaergaard, T. Salmi, V. Hänninen, and L. Halonen. The effect of large amplitude motions on the transition frequency redshift in hydrogen bonded complexes: A physical picture. *J. Chem. Phys.*, 140:184309, 2014.

[23] P. Jankowski, G. Murdachaew, R. Bukowski, O. Akin-Ojo, C. Leforestier, and K. Szalewicz. Ab initio water pair potential with flexible monomers. *J. Phys. Chem. A*, 119:2940–2964, 2015.

[24] K. Mackeprang, V. Hänninen, L. Halonen, and H. G. Kjaergaard. The effect of large amplitude motions on the vibrational intensities in hydrogen bonded complexes. *J. Chem. Phys.*, 142:094304, 2015.

[25] A. Mukhopadhyay, S. S. Xantheas, and R. J. Saykally. The water dimer II: Theoretical investigations. *Chem. Phys. Lett.*, 700:163–175, 2018.

[26]C. L. Vaillant, D. J. Wales, and S. C. Althorpe. Tunneling splittings from path-integral molecular dynamics using a Langevin thermostat. *J. Chem. Phys.*, 148:234102, 2018.

[27]X.-G. Wang and T. Carrington. Using monomer vibrational wavefunctions to compute numerically exact (12D) rovibrational levels of water dimer. *J. Chem. Phys.*, 148:074108, 2018.

[28]M. P. Metz, K. Szalewicz, J. Sarka, R. Tóbiás, A. G. Császár, and E. Mátyus. Molecular dimers of methane clathrates: ab initio potential energy surfaces and variational vibrational states. *Phys. Chem. Chem. Phys.*, 21:13504–13525, 2019.

[29]A. Nandi, C. Qu, P. L. Houston, R. Conte, Q. Yu, and J. M. Bowman. A CCSD(T)-based 4-body potential for water. *J. Phys. Chem. Lett.*, 12:10318–10324, 2021.

[30]L. Pauling. *The Nature of the Chemical Bond.* Cornwall University Press, New York, 1939.

[31]H. C. Longuet-Higgins. The symmetry groups of non-rigid molecules. *Mol. Phys.*, 6:445–460, 1963.

[32]P. R. Bunker and P. Jensen. *Molecular Symmetry and Spectroscopy.* NRC Research Press, Ottawa, 2006.

[33]G. R. Low and H. G. Kjaergaard. Calculation of OH-stretching band intensities of the water dimer and trimer. *J. Chem. Phys.*, 110(18):9104–9115, 1999.

[34]E. Vogt and H. G. Kjaergaard. Vibrational spectroscopy of the water dimer at jet-cooled and atmospheric temperatures. *Ann. Rev. Phys. Chem.*, 73:in press, 2022.

[35]E. Sälli, T. Salmi, and L. Halonen. Computational high-frequency overtone spectra of the water–ammonia complex. *J. Phys. Chem. A*, 115:11594–11605, 2011.

[36]E. Mátyus, G. Czakó, and A. G. Császár. Toward black-box-type full- and reduced-dimensional variational (ro)vibrational computations. *J. Chem. Phys.*, 130:134112, 2009.

[37]C. Fábri, E. Mátyus, and A. G. Császár. Rotating full- and reduced-dimensional quantum chemical models of molecules. *J. Chem. Phys.*, 134:074105, 2011.

[38]C. Fábri, M. Quack, and A. G. Császár. On the use of nonrigid-molecular symmetry in nuclear-motion computations employing a discrete variable representation: a case study of the bending energy levels of CH_5^+. *J. Chem. Phys.*, 147:134101, 2017.

[39]B. Podolsky. Quantum-mechanically correct form of Hamiltonian function for conservative systems. *Phys. Rev.*, 32:812–816, 1928.

[40]E. B. Wilson Jr., J. C. Decius, and P. C. Cross. *Molecular vibrations: the theory of infrared and Raman vibrational spectra.* McGraw Hill, New York, 1955.

[41]J. H. Frederick and C. Woywod. General formulation of the vibrational kinetic energy operator in internal bond-angle coordinates. *J. Chem. Phys.*, 111:7255–7271, 1999.

[42]T. B. Adler, G. Knizia, and H.-J. Werner. A simple and efficient CCSD(T)-F12 approximation. *J. Chem. Phys.*, 127:221106, 2007.

[43]K. A. Peterson, T. B. Adler, and H.-J. Werner. Systematically convergent basis sets for explicitly correlated wavefunctions: The atoms H, He, B–Ne, and Al–Ar. *J. Chem. Phys.*, 128:084102, 2008.

[44]H.-J. Werner, P. J. Knowles, F. R. Manby, J A. Black, K. Doll, A. Heßelmann, D. Kats, A. Köhn, T. Korona, D. A. Kreplin, Q. Ma, T. F. Miller, A. Mitrushchenkov, K. A. Peterson, I. Polyak, G. Rauhut, and M. Sibaev. The Molpro quantum chemistry package. *J. Chem. Phys.*, 152:144107, 2020.

[45]T. R. Dyke. Group theoretical classification of the tunneling–rotational energy levels of water dimer. *J. Chem. Phys.*, 66:492–497, 1977.

[46]A. G. Császár, C. Fábri, T. Szidarovszky, E. Mátyus, T. Furtenbacher, and G. Czakó. The fourth age of quantum chemistry: molecules in motion. *Phys. Chem. Chem. Phys.*, 14:1085–1106, 2012.

[47]D. O. Harris, G. G. Engerholm, and W. D. Gwinn. Calculation of matrix elements for one-dimensional quantum-mechanical problems and the application to anharmonic oscillators. *J. Chem. Phys.*, 43:1515–1517, 1965.

[48]J. V. Lill, G. A. Parker, and J. C. Light. Discrete variable representations and sudden models in quantum scattering theory. *Chem. Phys. Lett.*, 89:483–489, 1982.

[49]J. C. Light, I. P. Hamilton, and J. V. Lill. Generalized discrete variable approximation in quantum mechanics. *J. Chem. Phys.*, 82:1400–1409, 1985.

[50]Z. Bačić and J. C. Light. Theoretical methods for rovibrational states of floppy molecules. *Annu. Rev. Phys. Chem.*, 40:469–498, 1989.

[51]V. Szalay. Discrete variable representations of differential operators. *J. Chem. Phys.*, 99:1978–1984, 1993.

[52]J. M. Bowman, T. Carrington, and H.-D. Meyer. Variational quantum approaches for computing vibrational energies of polyatomic molecules. *Mol. Phys.*, 106:2145–2182, 2008.

[53]C. Lanczos. An iteration method for the solution of the eigenvalue problem of linear differential and integral operators. *J. Res. Natl. Bur. Stand.*, 45:255–282, 1950.

[54]G. Brocks, A. van der Avoird, B. T. Sutcliffe, and J. Tennyson. Quantum dynamics of non-rigid systems comprising two polyatomic fragments. *MolPhys*, 50(5):1025–1043, 1983.

[55]H. G. Kjaergaard, A. L. Garden, G. M. Chaban, R. B. Gerber, D. A. Matthews, and J. F. Stanton. Calculation of vibrational transition frequencies and intensities in water dimer: Comparison of different vibrational approaches. *J. Phys. Chem. A*, 112:4324–4335, 2008.

[56]E. Arunan, G. R. Desiraju, R. A. Klein, J. Sadlej, S. Scheiner, I. Alkorta, D. C. Clary, R. H. Crabtree, J. J. Dannenberg, P. Hobza, H. G. Kjaergaard, A. C. Legon, B. Mennucci, and D. J. Nesbitt. Definition of the hydrogen bond (IUPAC recommendations 2011). *Pure Appl. Chem.*, 83:1637–1641, 2011.

[57]A. S. Hansen, E. Vogt, and H. G. Kjaergaard. Gibbs energy of complex formation – combining infrared spectroscopy and vibrational theory. *Int. Rev. Phys. Chem.*, 38(1):115–148, 2019.

[58]A. L. Garden, L. Halonen, and H. G. Kjaergaard. Calculated band profiles of the OH-stretching transitions in water dimer. *J. Phys. Chem. A*, 112(32):7439–7447, 2008.

[59]Z. S. Huang and R. E. Miller. High-resolution near-infrared spectroscopy of water dimer. *J. Chem. Phys.*, 91(11):6613–6631, 1989.

[60]F. Huisken, M. Kaloudis, and A. Kulcke. Infrared spectroscopy of small size-selected water clusters. *J. Chem. Phys.*, 104:17–25, 1996.

[61]J. B. Paul, R. A. Provencal, C. Chapo, K. Roth, R. Casaes, and R. J. Saykally. Infrared cavity ringdown spectroscopy of the water cluster bending vibrations. *J. Phys. Chem. A*, 103(16):2972–2974, 1999.

[62]U. Buck and F. Huisken. Infrared spectroscopy of size-selected water and methanol clusters. *Chem. Rev.*, 100:3863–3890, 2000.

[63]I. León, R. Montero, F. Castaño, A. Longarte, and J. A. Fernández. Mass-resolved infrared spectroscopy of complexes without chromophore by nonresonant femtosecond ionization detection. *J. Phys. Chem. A*, 116:6798–6803, 2012.

[64]K. E. Otto, Z. Xue, P. Zielke, and M. A. Suhm. The raman spectrum of isolated water clusters. *Phys. Chem. Chem. Phys.*, 16:9849–9858, 2014.

[65]T. A. Ruden, T. Helgaker, P. Jørgensen, and J. Olsen. Coupled-cluster connected quadruples and quintuples corrections to the harmonic vibrational frequencies and equilibrium bond distances of HF, N2, F2, and CO. *J. Chem. Phys.*, 121(12):5874–5884, 2004.

[66]G. Rauhut, G. Knizia, and H.-J. Werner. Accurate calculation of vibrational frequencies using explicitly correlated coupled-cluster theory. *J. Chem. Phys.*, 130(5):054105, 2009.

[67]J. R. Lane and H. G. Kjaergaard. XH-stretching overtone transitions calculated using explicitly correlated coupled cluster methods. *J. Chem. Phys.*, 132(17):174304, 2010.